Geophys. J. Int. (0000) **000**, 000–000

Supplement: Stabilized mascon solutions through combinations of GRACE and SLR normal equations

M. J. Croteau[1], B. D. Loomis[1], and T. J. Sabaka[1]
[1] *Geodesy and Geophysics Laboratory, NASA Goddard Space Flight Center, Greenbelt, MD, USA*

6 January 2025

S1 FAST MASCON FORMULATION AND PARAMETERIZATION

In this study, we followed the same mascon formulation and parameterization as in (Croteau et al., 2021) and estimate GRACE-only and GRACE+SLR solutions for April 2002 through July 2023. This means that the GRACE-only solution examined here is simply an extension of the mascon solution presented in that paper to include 25 additional months. Since both solutions use the same regularization design as that paper, differences in the recovered solutions will show the effects of including SLR information while holding other variables fixed. In this section, we repeat the major design decisions from that paper for reference here.

As in (Croteau et al., 2021), we define the regularization matrix in covariance space as $\mathbf{P}^{-1}$, and define the individual terms for each row/mascon i and column/mascon j as $P_{i,j} = \rho_{ij}\sigma_i\sigma_j$. As before, we use the same set of 41,168 1-arc-degree mascons as already commonly used in the GSFC RL06 mascon solution. We use the same map of expected uncertainties, σ_i, shown in Fig. S1. Correlations for each mascon i, j pair, ρ_{ij}, are defined using the Gaussian smoothing function for a 300 km radius, with regional constraints applied to set $\rho_{ij} = 0$ if mascons i and j are in separate geographic regions. Regions included in the regularization design include: (1) Greenland Ice Sheet, low elevations ($<$ 2000 m), (2) Greenland Ice Sheet, high elevations ($>$ 2000 m), (3) Antarctic Ice Sheet including the Ronne and Ross ice shelves, (4) Gulf of Alaska, (5) Land, (6) Ocean, including smaller ice shelves, (7) Mediterranean Sea, (8) Black Sea, (9) Red Sea, (10) Caspian Sea, and (11) Hudson Bay.

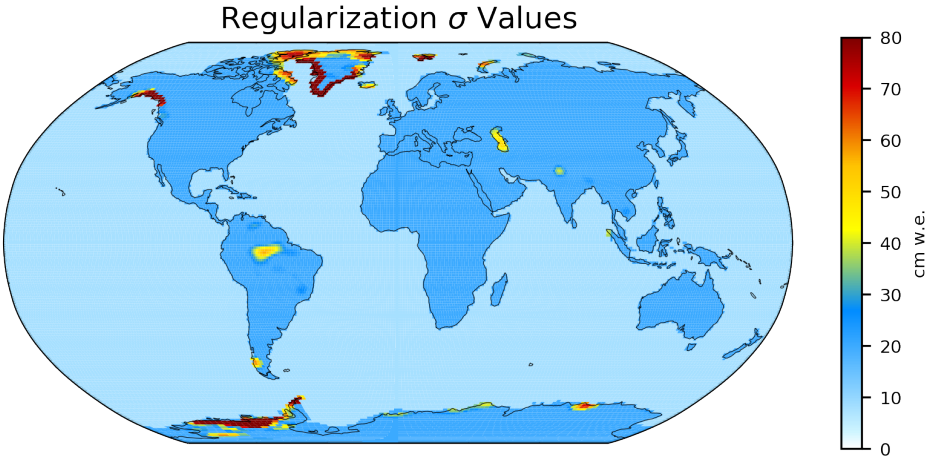

Figure S1. Expected uncertainties σ's used to populated the regularization matrix (from Croteau et al., 2021).

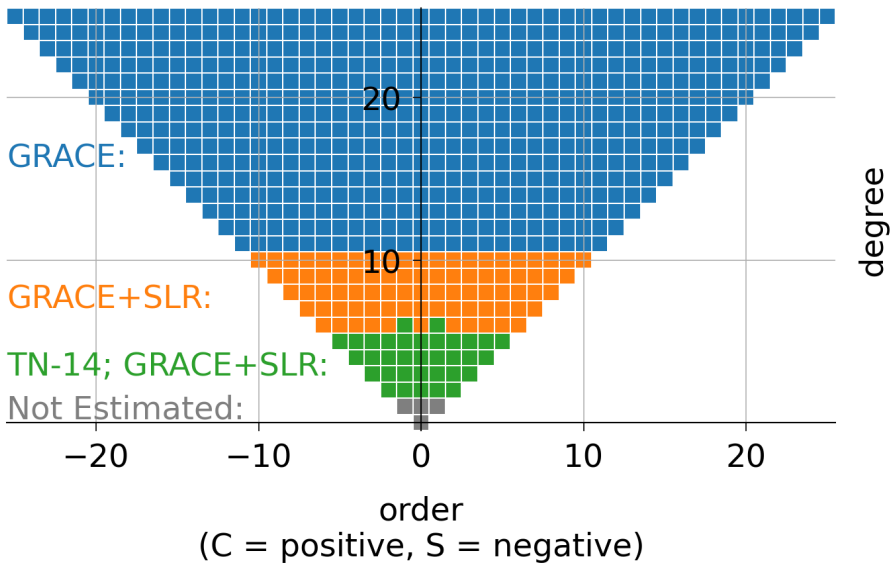

Figure S2. Spherical harmonic coefficients included in the estimate per source (through degree/order 25). Also depicted are those coefficients included in the TN-14 SLR-only estimate of $C_{2,0}$ and $C_{3,0}$.

S2 SPHERICAL HARMONIC COEFFICIENT BREAKDOWN

The combined GRACE+SLR solution includes estimates of gravity field spherical harmonic coefficients from GRACE(-FO) for degrees 2-96 and from SLR for degrees 2-10. This means the combination includes a larger spherical harmonic expansion from SLR than is used in developing the SLR-only "GRACE Technical Note 14" estimates of $C_{2,0}$ and $C_{3,0}$, which is estimated from only coefficients in degrees 2-5 plus $C_{6,1}$ and $S_{6,1}$ for stability reasons. Degree 0 (Earth's total mass) and 1 (Earth's geocenter) coefficients are not included in the estimate, as typical for GRACE solutions, and Degree 1 terms are instead restored after the estimation step following (Sun et al., 2016). This breakdown is shown in Fig. S2.

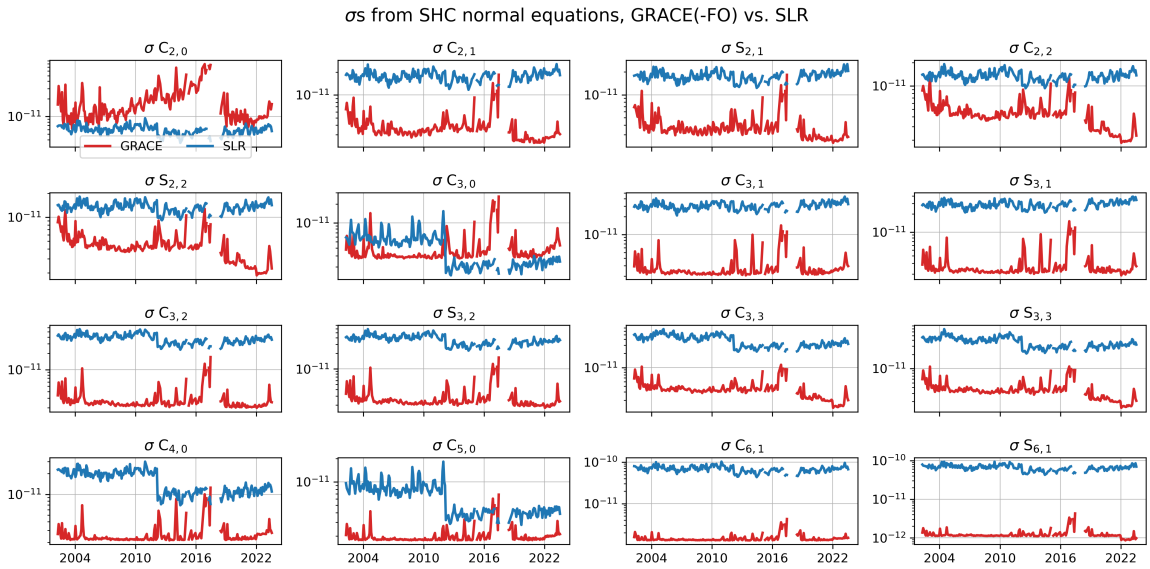

Figure S3. Spherical harmonic σs from the GRACE (red) and SLR (blue) variance-covariance matrices. Smaller values indicate that data type contributes more to the combination, meaning $C_{2,0}$ is primarily resolved by SLR, as is $C_{3,0}$ after the 2012 launch of LARES.

S3 GRACE AND SLR CONTRIBUTIONS TO FINAL COMBINATION

As described in Section 2.2, we determined that SLR should be up-weighted by a factor of 10 relative to GRACE in the combination solution, so that $C_{2,0}$ and (after the launch of LARES in 2012) $C_{3,0}$ will be driven by SLR in the combination. To demonstrate the effects of this weighting, we computed the variance-covariance matrix for each data type at each time by inverting the weighted GRACE and SLR normal matrices and plotted the σ values for both data types in Fig. S3.

To illustrate the extent to which each data type contributes to each spherical harmonic term, we compute resolution matrices for GRACE and SLR ($\mathbf{R}_G$ and $\mathbf{R}_S$) from their respective normal matrices for GRACE and SLR ($\mathbf{N}_G$ and $\mathbf{N}_S$) following the procedure in (Sneeuw et al., 2000) and (Meyer et al., 2019), where $\mathbf{N} = w_G\mathbf{N}_G + w_S\mathbf{N}_S$, by

$$\begin{aligned} \mathbf{R}_G &= \mathbf{N}^{-1}\mathbf{N}_G, \\ \mathbf{R}_S &= \mathbf{N}^{-1}\mathbf{N}_S. \end{aligned} \tag{1}$$

The diagonal terms of these matrices provide the relative contributions of each data type, where a value of 1 means that the combination is entirely determined by that data type and 0 means that data type has no influence on the combination. Since we are comparing two data types, $\mathbf{R}_G = \mathbf{I} - \mathbf{R}_S$ and we can evaluate the contributions of both types by considering only one matrix. Fig. S4 shows the diagonal terms from $\mathbf{R}_G$, meaning terms with values close to 1 are driven by GRACE and those with values close to 0 are driven by SLR. We see that the influence of SLR varies in time due to both the inclusion of new SLR satellites (e.g., after the 2012 launch of LARES) and the quality of GRACE/SLR data over time (e.g., Feb vs. Mar 2015).

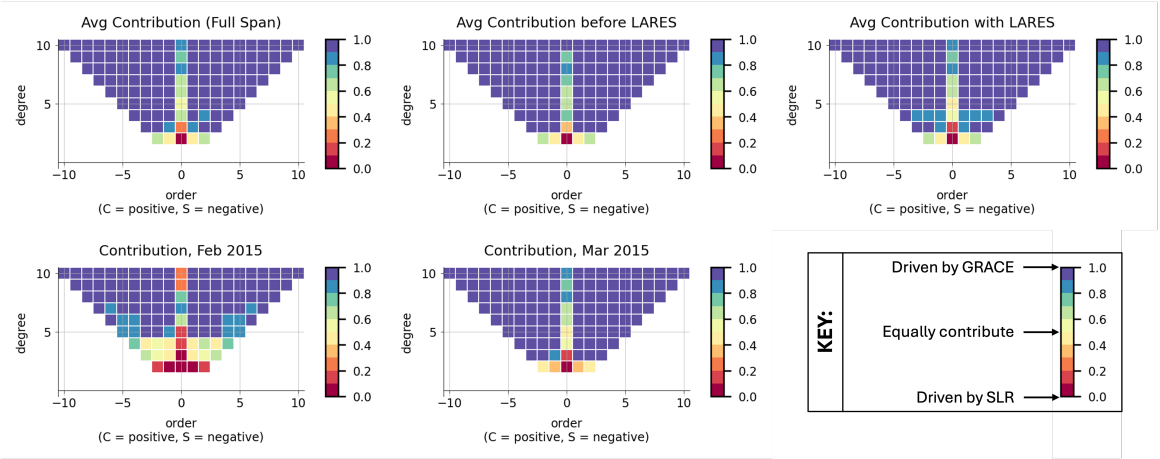

Figure S4. Contributions per spherical harmonic coefficient from GRACE and SLR for portions of the combination time span. Here a contribution of "1" indicates that the coefficient is driven by GRACE, "0" indicates that the coefficient is driven by SLR, and values in between are driven by GRACE and SLR in proportion to the value.

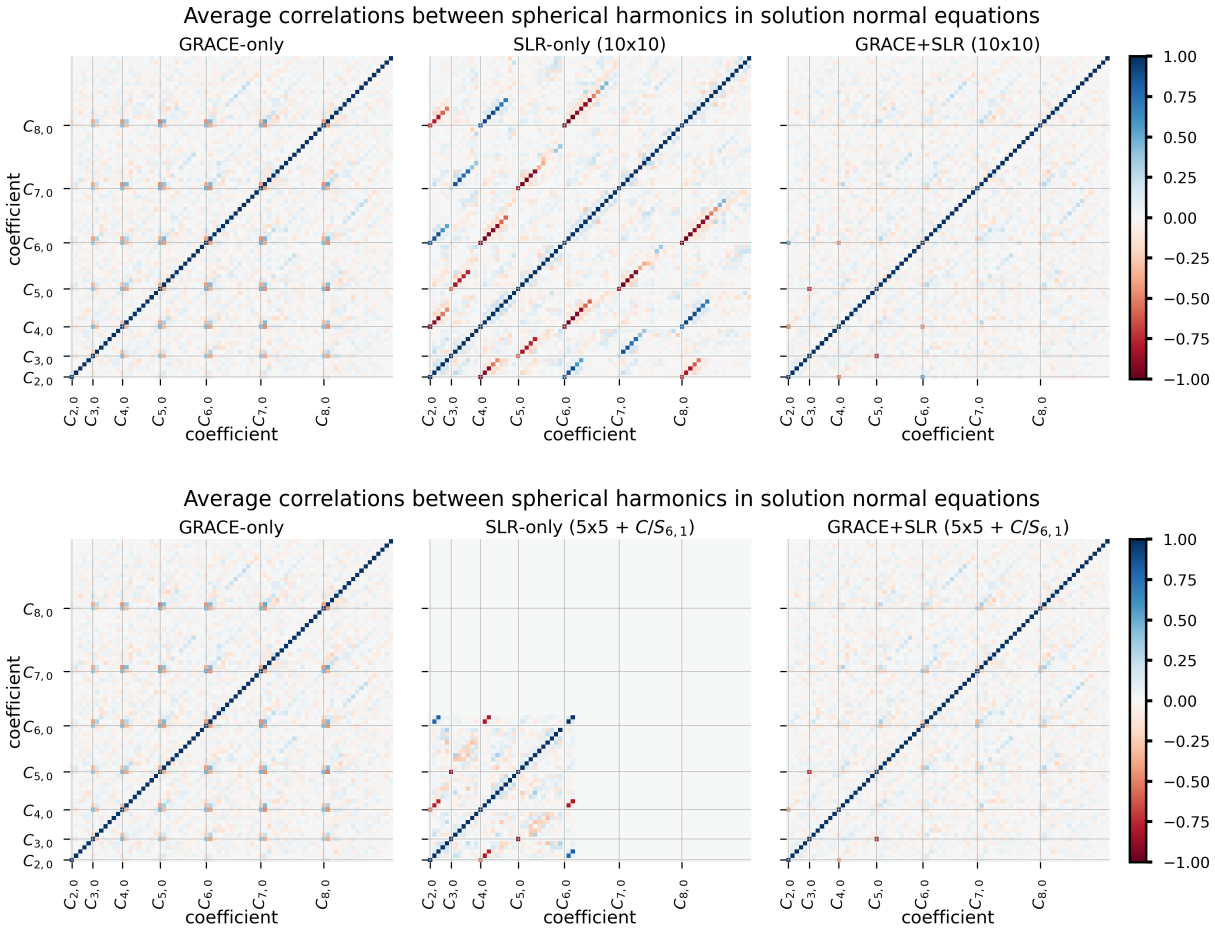

Figure S5. Average correlations between spherical harmonic coefficients in GRACE-only, SLR-only, and GRACE+SLR solutions for SLR solutions to degree/order 10 and truncated to degree/order 5 plus $C_{6,1}$ and $S_{6,1}$.

S4 EFFECTS OF CHOICE OF SLR PARAMETERS

For the SLR solution in our combination, we include normal equations for a spherical harmonic expansion to degree/order 10, whereas GRACE TN-14 (derived from the same SLR normal equations) only includes normal equation information for harmonics to degree/order 5 plus those for $C_{6,1}$ and $S_{6,1}$. The SLR-only solution in TN-14 limits which higher order terms are included to minimize correlations between $C_{2,0}$ and $C_{3,0}$ and other higher-order terms in the SLR-only solution. Importantly, TN-14 use of a reduced SLR expansion represents a trade-space that must be done for an SLR-only solution to produce the least problematic recovery of $C_{2,0}$ and $C_{3,0}$, and the exact subset of coefficients to include in that expansion has been subject to debate and revision over time.

We tested combination solutions using both a full degree 10 expansion and the reduced expansion from TN-14 for SLR. We found that both GRACE+SLR combinations resolved correlation issues similarly through degree 5, while the full expansion did a slightly better job beyond degree 5. Fig. S5 shows a comparison of the resultant correlations between coefficients for a GRACE+SLR solution with the full and truncated SLR expansions. Ultimately, choosing to use the full degree 10 expansion for SLR allows SLR to more fully contribute to the combination while simultaneously removing the trade-space question of which coefficients to include in a reduced expansion from factoring into the GRACE+SLR combination.

S5 UNCERTAINTY QUANTIFICATION METHOD

In this study, we follow the same method for GRACE mascon uncertainty quantification (both noise and bias due to leakage) as developed in (Loomis et al., 2019a; Croteau et al., 2020). This uses a data-driven approach to estimating solution noise, and applies the resolution operator in estimating bias due to the regularization. Here we provide a brief summary of that method, but a full description and rationale is in Section 2.4 of (Loomis et al., 2019a).

S5.1 Noise covariance

First, we define a noise matrix, $\hat{\mathbf{n}} \in \mathcal{R}^{M\times N}$ (where M is the number of months in the solution and N is the number of mascons), as the difference between our solution and one that has been temporally filtered,

$$\hat{\mathbf{n}} \equiv \hat{\mathbf{x}} - \mathcal{F}(\hat{\mathbf{x}}), \tag{2}$$

where $\mathcal{F}()$ is a second-order Savitzky-Golay filter selected to match the noise level predicted by the post-fit observation residuals. Assuming $\mathbb{E}[\hat{n}] = 0$, the spatial error covariance, $\mathbf{C}_s \in \mathcal{R}^{N\times N}$, and temporal error covariance, $\mathbf{C}_t \in \mathcal{R}^{M\times M}$, are

$$\begin{aligned} \mathbf{C}_s &= \frac{1}{M-1}\hat{\mathbf{n}}^{\mathrm{T}}\hat{\mathbf{n}} \\ \mathbf{C}_t &= \frac{1}{N-1}\hat{\mathbf{n}}\hat{\mathbf{n}}^{\mathrm{T}}. \end{aligned} \tag{3}$$

We define a spatial scale $\mathbf{S} \in \mathcal{R}^{N\times 1}$ for each kth mascon as $\mathbf{S}(k) \equiv \sqrt{\mathbf{C}_s(k,k)}$ and a time scale $\mathbf{T} \in \mathcal{R}^{M\times 1}$ for each ith month as $\mathbf{T}(i) \equiv \sqrt{\mathbf{C}_t(i,i)}$, and then approximate the spatiotemporal noise $\hat{\sigma} \in \mathcal{R}^{M\times N}$ as the outer product of these terms,

$$\hat{\sigma} = \mathbf{T}\mathbf{S}^{\mathrm{T}}. \tag{4}$$

S5.2 Mascon bias (or leakage)

The regularized mascon solution bias provides a measure of the difference between the true state and the regularized estimate. While the true state is unknown, the best estimate $\hat{\mathbf{x}}_i$ at time i can be used to approximate bias by

$$\hat{\ell}_i = (\mathbf{I} - \mathbf{R}_i)\hat{\mathbf{x}}_i, \tag{5}$$

where $\mathbf{R}$ is the resolution operator,

$$\mathbf{R} = \left(\mathbf{A}^{\mathrm{T}}\mathbf{W}\mathbf{A} + \mathbf{P}\right)^{-1}\left(\mathbf{A}^{\mathrm{T}}\mathbf{W}\mathbf{A}\right) \tag{6}$$

or for fast mascons (Croteau et al., 2021),

$$\mathbf{R} = \mathbf{P}^{-1}\mathbf{L}^{\mathrm{T}}\left(\lambda\mathbf{N}^{-1} + \mathbf{L}\mathbf{P}^{-1}\mathbf{L}^{\mathrm{T}}\right)\mathbf{L}, \tag{7}$$

$\mathbf{A} \equiv \mathbf{H}\mathbf{L}$, $\mathbf{H}$ is the partial derivative matrix of range rate measurements with respect to the differential spherical harmonic expansion, $\mathbf{L}$ is the partial derivative matrix of the differential spherical harmonic coefficients with respect to the mascons, and $\lambda\mathbf{P}^{-1}$ is the scaled signal covariance from Section S1.

The full set of bias estimates $\hat{\ell}$ contains both a deterministic (or trend) component and a stochastic component, which we split as $\hat{\ell} = \hat{\ell}_{\mathrm{trend}} + \hat{\ell}_{other}$ and $\hat{\ell}_{\mathrm{trend}}$ is computed as the best fit trend of $\hat{\ell}$.

Since bias for each time t from Eq. 5 are determined from the best estimate, we do not use the individual $\ell_{\mathrm{other},i}$ biases directly in our error budget but instead compute for each mascon the standard deviation of these biases over time to determine a more representative approximation of stochastic bias, which we call $\hat{\ell}_\sigma$.

S5.3 Complete mascon error budget

The total 95% uncertainty for the set of mascons is then determined from the noise covariance and the bias trend and stochastic terms as

$$\varepsilon_{\mathrm{mascon}} = \left|\hat{\ell}_{\mathrm{trend}}\right| + 2\left(\hat{\ell}_\sigma + \hat{\sigma}\right). \tag{8}$$

Similarly, we can determine the 95% uncertainty for a region (accounting for both correlations between mascons within a region) as

$$\varepsilon_{\mathrm{region}} = |\overline{\hat{\ell}_{\mathrm{trend}}}| + \frac{2(\overline{\hat{\ell}_\sigma} + \overline{\hat{\sigma}})}{\sqrt{n_{\mathrm{region}}/z}} \tag{9}$$

where n_{region} is the number of mascons within the region and z is a measure of spatial resolution. Following the procedure in (Loomis et al., 2019a), we determined that $z = 20$ for all land locations and seas and $z = 30$ for the open ocean.

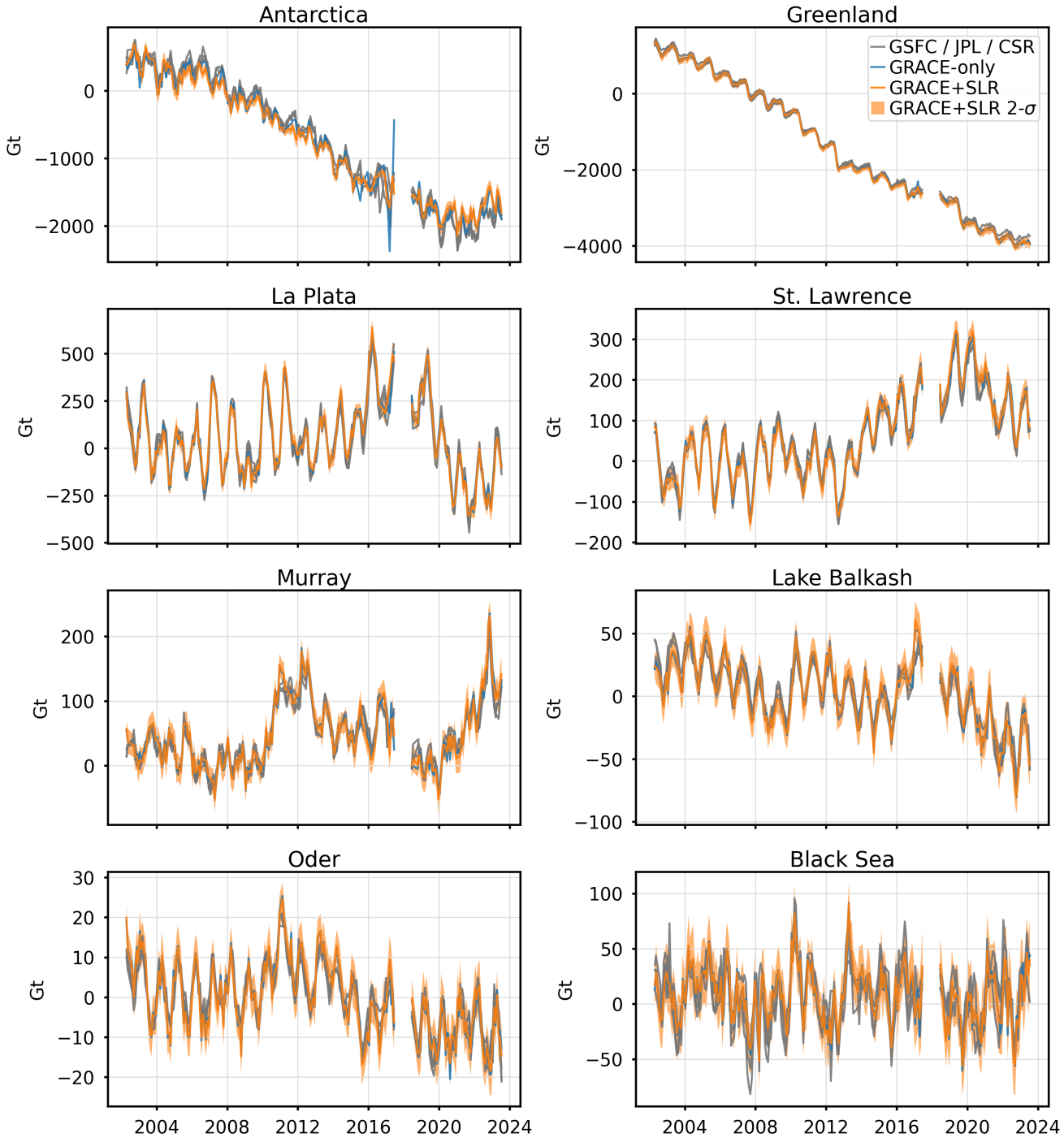

Figure S6. Basin mass change recovered from GRACE+SLR and GRACE-only solutions, with the GSFC, JPL, and CSR mascon solutions shown in gray for comparison. For most months and basins, the inclusion of SLR has only small impacts on the recovered signal but has larger impacts in the reduction of the error of that signal.

S6 BASIN MASS CHANGE COMPARISONS

Basin mass change was computed for numerous basins varying in size and type (including ice covered, land, and seas) for both the GRACE-only and GRACE+SLR mascons. Fig. S6 show few substantial changes in the recovered basin trends, annual signals, or inter-annual signals using the GRACE+SLR solution compared to the GRACE-only solution, though signals in Antarctica in particular do show notable improvements for individual months. We additionally see very good agreement with both solutions for all basins when comparing to the commonly available mascon solutions from GSFC, JPL, and CSR.

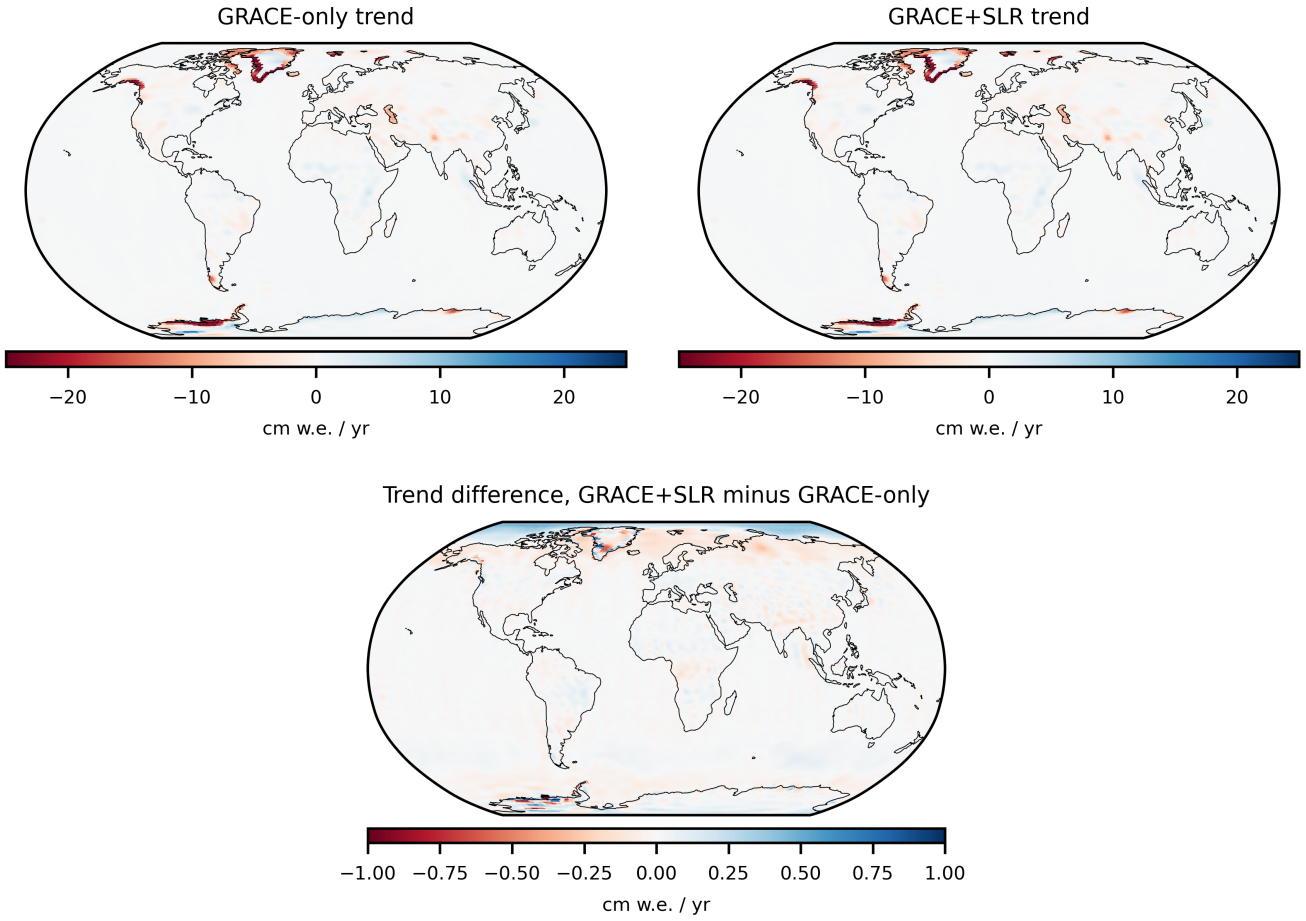

Figure S7. Maps of recovered trends from GRACE-only and GRACE+SLR, as well as the difference between the two.

Additionally, we computed maps of the recovered mascon trends from GRACE+SLR and GRACE-only. Figure S7 shows the global trend for each as well as a trend difference map of GRACE+SLR minus GRACE. We see only small changes in trend due to the GRACE+SLR combination, and nearly all changes are differences in how regional trends are recovered locally, likely due to the reduction in noise shown in Table 1. The one wider-scale change that can be seen is over the Arctic Ocean, where the GRACE+SLR solution shows a more positive trend across large portions of that basin along with a corresponding decrease in trend in the vicinity of Greenland and Scandinavia.

REFERENCES

Croteau, M.J., Nerem, R.S., Loomis, B.D., & Sabaka, T.J., 2021. Development of a Daily GRACE Mascon Solution for Terrestrial Water Storage. *J. Geophys. Res. Solid Earth*, 125, e2019JB018468, https://doi.org/10.1029/2019JB018468.

Croteau, M.J., Sabaka, T.J., & Loomis, B.D., 2021. GRACE fast mascons from spherical harmonics and a regularization design trade study. *J. Geophys. Res. Solid Earth*, 126, e2021JB022113, https://doi.org/10.1029/2021JB022113.

Loomis, B.D., Luthcke, S.B. & Sabaka, T.J., 2019. Regularization and error characterization of GRACE mascons. *J. Geod.*, 93, 1381–1398, https://doi.org/10.1007/s00190-019-01252-y.

Meyer, U., Sosnica, K., Arnold, D., Dahle, C., Thaller, D., Dach, R., & Jäggi, A., 2019. SLR, GRACE and Swarm Gravity Field Determination and Combination. *Remote Sens.*, 11, 956, https://doi.org/10.3390/rs11080956.

Sneeuw, N. A Semi-Analytical Approach to Gravity Field Analysis From Satellite Observations; Deutsche Geodätische Kommission, C 527: München, Germany, 2000; ISBN 3-7696-9566-6.

Sun, Y., Riva, R., and Ditmar, P., 2016. Optimizing estimates of annual variations and trends in geocenter motion and J2 from a combination of GRACE data and geophysical models. *J. Geophys. Res. Solid Earth*, 121, 8352–8370, https://doi.org/10.1002/2016JB013073.